Coupled spin-charge dynamics in magnetic van der Waals heterostructures

Avinash Rustagi,[1,*] Abhishek Bharatbhai Solanki,[1] Yaroslav Tserkovnyak,[2] and Pramey Upadhyaya[1,†]
[1]*School of Electrical and Computer Engineering, Purdue University, West Lafayette, Indiana 47907, USA*
[2]*Department of Physics and Astronomy, University of California, Los Angeles, California 90095, USA*

(Received 2 December 2019; accepted 1 September 2020; published 18 September 2020)

We present a phenomenological theory for coupled spin-charge dynamics in magnetic van der Waals (vdW) heterostructures. The system studied consists of a layered antiferromagnet inserted into a capacitive vdW heterostructure. It has been recently demonstrated that charge doping in such layered antiferromagnets can modulate the strength, and even the sign, of exchange coupling between the layer magnetizations. This provides a mechanism for electrically generating magnetization dynamics. The central result we predict here is that the magnetization dynamics reciprocally results in inducing charge flows. Such dynamics makes magnetic van der Waals heterostructures interesting candidates for spintronics applications. To this end, we also show that these systems can be used to convert subterahertz-radiation-induced magnetization dynamics into electrical signals.

DOI: 10.1103/PhysRevB.102.094421

I. INTRODUCTION

Two-dimensional (2D) magnetism offers opportunities to investigate phenomena driven by enhanced fluctuations, reduced symmetries, and nontrivial topology [1]. The recent discovery of magnetic order in few-layer systems held together by van der Waals forces (magnetic vdW [2,3]) have thus emerged as a promising avenue for fundamental research and technological applications. Furthermore, by taking advantage of layer-by-layer assembly, magnetic vdW can be interfaced with a wide range of materials to form heterostructures with desired functionality [4].

A functionality of fundamental interest is the ability to interconvert between spin and charge degrees of freedom. Such spin-charge conversion has been a key enabler of spintronics technology, which has attracted rigorous interest as an alternative to charge-based technology [5,6]. Consequently, a number of fundamental phenomena allowing for conversion between spin and charge has been uncovered in the recent past, which includes reciprocal pairs such as spin torque-spin pumping [7–10], the spin Hall–inverse spin Hall effect [11–14], the Rashba Edelstein–inverse Rashba Edelstein effect [15–17], and the direct-converse magnetoelectric effect [18,19]. The search for alternative low-dissipation mechanisms and material platforms for efficient conversion between spin and charge is an active area of research [6].

Bilayer chromium iodide (CrI_3)-based vdW heterostructures have recently emerged as one such platform. CrI_3 is a vdW magnet with ferromagnetically ordered layers coupled via an antiferromagnetic interlayer coupling [20,21]. The interlayer coupling is sensitive to charge residing on each layer. This has been utilized to switch the ground-state spin configuration in gated bilayer CrI_3 heterostructures between a layered antiferromagnetic and a ferromagnetic state electrically [22]. Reciprocity then dictates the existence of an inverse mechanism, wherein the charge distribution in the same heterostructure can be modulated by inducing magnetization dynamics. Furthermore, the large out-of-plane anisotropy, in combination with the antiferromagnetic coupling, gives rise to subterahertz antiferromagnetic resonance (AFMR) modes in the absence of external magnetic fields [23,24]. This suggests the existence of a new reciprocal pair in gated bilayer CrI_3 heterostructures, which is capable of interconverting between spin and charge up to subterahertz frequencies. In this paper, we thus present a phenomenological theory of dynamical spin-charge coupling in vdW heterostructures involving bilayer CrI_3. In particular, we predict the phenomena of charge pumping by magnetization dynamics, which can be utilized for electrical detection of AFMR or converting gigahertz to subterahertz radiation into an electrical signal.

II. STRUCTURE AND MODEL

Motivated by recent experiments [22], here we consider a bilayer CrI_3 system inserted into a capacitor formed by hexagonal boron nitride (h-BN), which is contacted by metal layers as shown in the top panel of Fig. 1. The CrI_3 layers are themselves connected to ground (for example via contacting them by graphene layers). The ferromagnetically ordered layers are coupled via antiferromagnetic exchange [20,23]. Moreover, the magnetization of the layers has an out-of-plane easy axis, which arises due to anisotropic exchange interaction [24]. Thus, the free energy per unit area within the macrospin approximation in its minimal form consists of an easy-axis uniaxial anisotropy and an antiferromagnetic interlayer exchange,

$$\mathcal{F}(\vec{m}_1, \vec{m}_2) = -Km_{1z}^2 - Km_{2z}^2 + J_\perp \vec{m}_1 \cdot \vec{m}_2. \qquad (1)$$

The charges on the CrI_3 layers couple to the magnetic degrees of freedom giving rise to additional free energy $\mathcal{F}(\vec{m}_i, \sigma_i)$ terms. The functional form of $\mathcal{F}(\vec{m}_i, \sigma_i)$ is dictated by the time-reversal and structural symmetry of our vdW

*arustag@purdue.edu
†prameyup@purdue.edu

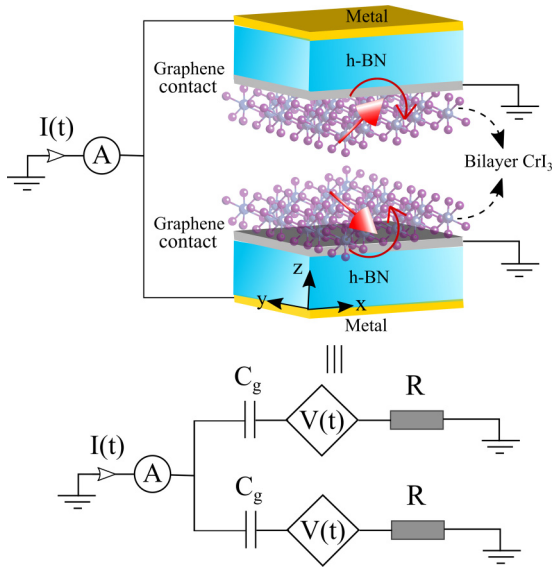

FIG. 1. Schematic of the grounded (using graphene contacts) bilayer CrI_3 inserted into a h-BN capacitor for coupled spin-charge dynamics. Effective circuit model for the device structure accounting for the magnetization-dynamics-induced charge dynamics.

heterostructure. In particular, our structure has inversion symmetry under which the symmetric charge combination $\sigma_1 + \sigma_2$ remains invariant, while the antisymmetric charge combination $\sigma_1 - \sigma_2$ changes sign. Noting that the magnetization $\vec{m}$ is not affected by structural inversion, the coupling between the magnetic and charge degrees of freedom to the lowest order in σ_i, and obeying structural inversion and time reversal, can be written as [25]

$$\mathcal{F}(\vec{m}_i, \sigma_i) = -\lambda\,(\sigma_1 + \sigma_2)\vec{m}_1 \cdot \vec{m}_2. \tag{2}$$

This can be identified as doping-induced change in interlayer exchange coupling. Its strength is parametrized by λ (energy per unit charge), which for CrI_3 is $\sim$mV, allowing for the switching of magnetic order since $\lambda(\sigma_1 + \sigma_2)$ is comparable to the interlayer exchange $J_\perp$ [22]. The order of magnitude of such a doping-induced exchange energy modification is on par with other spin-charge coupling mechanisms studied for electrical control of magnetic order (e.g., voltage-controlled magnetic anisotropy, or VCMA [26,27]) [28]. We highlight that the experimental observation that asymmetric charge does not induce changes in the interlayer exchange [22] can be directly related to the structural symmetry of the vdW heterostructure. Additionally, the asymmetric charge can also couple to the magnetic degrees of freedom via a term of the form $\sim\zeta(\sigma_1 - \sigma_2)(\vec{m}_1 - \vec{m}_2)\cdot\vec{H}$. This "magnetoelectric coupling" has recently been observed in experiments [20]. However, the magnetoelectric effect is found to be less efficient for inducing magnetization dynamics when compared with the doping-induced interlayer exchange [22]. Thus, here the spin-charge coupling is restricted to the form given by Eq. (2).

Experimentally, the coupling given by Eq. (2) has been utilized to electrically switch magnetic order [22]. Reciprocally, a change in the magnetic configuration should alter charge density on the CrI_3 layer. We next derive an equivalent circuit

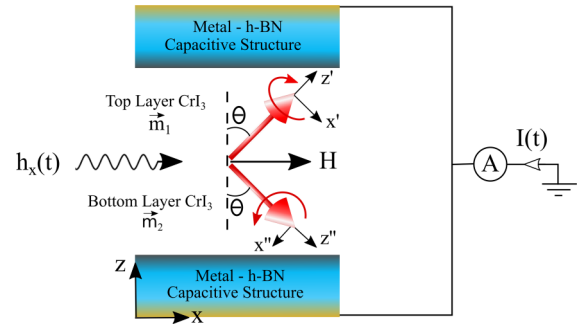

FIG. 2. Schematic of the proposed AFMR setup. The equilibrium magnetizations cant by an angle θ due to the applied dc magnetic field H and the AFMR mode is excited by the radiation field $h_x(t)$.

for this coupled spin-charge dynamics. To this end, we need to supplement Eqs. (1) and (2) with the electrical energy solely due to charges, which is given by

$$\mathcal{F}(\sigma_1, \sigma_2) = \frac{\sigma_1^2}{2C_g} + \frac{\sigma_2^2}{2C_g}. \tag{3}$$

Here, $C_g = \epsilon/d$ is the geometrical capacitance (per unit area) of the h-BN layer where ϵ and d are the permittivity and thickness of h-BN, respectively [29]. In Eq. (3), we have adopted the lumped-circuit model for describing charge dynamics, which is valid for the lateral dimensions of the studied heterostructures [30].

Collecting the free energy terms involving charge densities, we have

$$\mathcal{F}_\sigma = -\lambda(\sigma_1 + \sigma_2)\vec{m}_1 \cdot \vec{m}_2 + \frac{\sigma_1^2}{2C_g} + \frac{\sigma_2^2}{2C_g}. \tag{4}$$

Assuming R to be the series combination of the resistance of the external circuit and the resistance between graphene contacts and the CrI_3 layer, we can draw an effective circuit for the vdW heterostructure as shown in Fig. 1. The central result of this model is that a dynamic magnetization gives rise to a time-dependent voltage

$$V = -\partial\mathcal{F}(\vec{m}_i, \sigma)/\partial\sigma = \lambda\,\vec{m}_1 \cdot \vec{m}_2. \tag{5}$$

This circuit is the first main result of this paper.

III. CHARGE PUMPING

To demonstrate the effects of the reciprocal process of magnetization-dynamics-induced voltage, we propose to utilize the AFMR setup (see Fig. 2). In this case, the antiferromagnet is subjected to an electromagnetic radiation in the presence of a dc magnetic field. A resonant excitation of the magnetic order parameter occurs when the frequency of the electromagnetic radiation coincides with the frequency of the inherent magnetic dynamical modes of the antiferromagnet (which can be tuned by varying the strength of the dc magnetic field). The second main result of this paper is that in the CrI_3-based vdW heterostructures the absorbed radiation also gives rise to an electrical signal. In particular, when the RC time (time constant associated with the circuit given by the product of the circuit's resistance R and

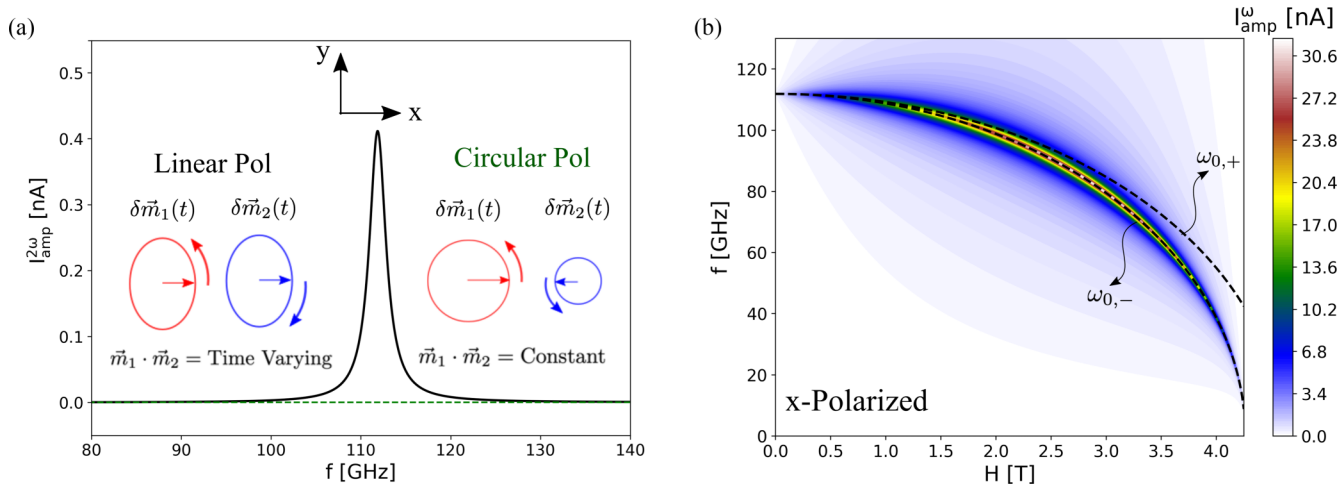

FIG. 3. (a) Electrical response ($I^{2\omega}_{amp}$) from Kittel modes at 2ω from magnetization dynamics induced by linearly (solid) and circularly (dashed) polarized radiation fields as a function of excitation field frequency in absence of dc field $H = 0$. The inset displays the precession of magnetization deviations transverse to the equilibrium orientation, of the top and bottom CrI_3 layers for both polarizations. (b) Evaluated current amplitude at excitation field frequency I^{ω}_{amp} as a function of excitation magnetic field frequency and the in-plane dc magnetic field for x-polarized excitation field. Dashed lines show the two AFMR modes [Eq. (8)] as a function of in-plane dc field.

capacitance C) associated with vdW heterostructure is smaller than the timescale associated with magnetization dynamics [31–34], the induced voltage results in a flow of charge current in the external circuit, which is given by

$$j_{ext}(t) = \dot{\sigma}_1 + \dot{\sigma}_2 = 2\lambda\, C_g\, \partial_t \vec{m}_1 \cdot \vec{m}_2. \tag{6}$$

We next calculate analytically the charge current pumped due to AFMR within the linear response, which is corroborated by numerical simulations.

The magnetization dynamics are governed by the Landau-Lifshitz-Gilbert (LLG) equation,

$$\dot{\vec{m}}_i = -\gamma\, \vec{m}_i \times [\vec{H}_{\text{eff},i} + \vec{H}_{\text{ext}} + \vec{h}_{\sim}] + \alpha\, \vec{m}_i \times \dot{\vec{m}}_i, \tag{7}$$

where the index $i = \{1, 2\}$ corresponds to the two layers, $\gamma > 0$ is the gyromagnetic ratio, α is the damping, $\vec{H}_{\text{eff},i} = -\partial_{\vec{m}_i}\mathcal{F}$, and $\vec{h}_{\sim}$ represents the ac excitation field. At elevated temperatures and/or when we are interested in thermal fluctuations, the appropriate stochastic Langevin field can be included in the LLG equation, as dictated by the fluctuation-dissipation theorem. For CrI_3, however, where electric control of a well-formed magnetic order has been demonstrated at ~4 K [22], we do not concern ourselves with the noise, at this point. We take the dc external field to be oriented along the x axis, $\vec{H}_{\text{ext}} = H\hat{x}$. This dc field cants the otherwise z-axis-oriented $\vec{m}_i$ to align with z', which makes a polar angle θ with the z axis (see Fig. 2). The polar angle satisfies $\sin\theta = H/(H_k + 2H_J)$ when $H < H_k + 2H_J$ and $\theta = \pi/2$ for $H > H_k + 2H_J$. Here $H_k = 2K/M_s$ is the anisotropy field and $H_J = J_\perp/M_s$ is the interlayer exchange field. The eigenmodes, found by solving the LLG linearized about the tilted equilibrium [35], correspond to the AFMR frequencies given by

$$\omega_{0,\pm} = \sqrt{[\omega_{\text{eq}} \pm \omega_J][\omega_{\text{eq}} \mp \omega_J \cos 2\theta - \omega_k \sin^2\theta]}, \tag{8}$$

where $\omega_k = \gamma H_k$, $\omega_J = \gamma H_J$, and $\omega_{\text{eq}} = \gamma H_{\text{eq}}$ are the frequencies corresponding to the anisotropy, interlayer exchange, and equilibrium fields. The equilibrium field experienced by the magnetizations has contributions from external, anisotropy, and interlayer exchange fields $H_{\text{eq}} = H\sin\theta + H_k\cos^2\theta + H_J\cos 2\theta$. The large easy-axis out-of-plane anisotropy in few-layer CrI_3, corresponding to a field of $H_k = 3.75$ T, results in a large spin-wave gap ~110 GHz [24] for $\theta = 0$. The presence of the in-plane dc field H lowers the AFMR frequency by effectively offsetting the out-of-plane anisotropy field. Also, the two Kittel modes that are degenerate in the absence of a dc field are now split (cf. Fig. 3).

To calculate the charge current pumped by the above modes, we need to find $\vec{m}_1 \cdot \vec{m}_2$ [cf. Eq. (6)]. For this purpose, we also evaluate the deviations transverse to the tilted equilibrium magnetizations (z' and z'' axis), $(\delta m'_{1x}, \delta m'_{1y})$ and $(\delta m''_{2x}, \delta m''_{2y})$, within the linearized LLG. A convenient choice for the solution is in terms of the collective coordinates $X_\pm = \delta m'_{1x} \pm \delta m''_{2x}$ and $Y_\pm = \delta m'_{1y} \pm \delta m''_{2y}$, which gives

$$\vec{m}_1 \cdot \vec{m}_2 \approx \sum_{s=\pm} s\frac{Y_s^2 - \cos 2\theta\left(X_s^2 + 2s\right)}{4} + \sin 2\theta X_-, \tag{9}$$

where

$$\begin{aligned}\begin{pmatrix} X_+ \\ Y_+ \end{pmatrix} &= \text{Re}\left[\frac{2\gamma\, h_y e^{-i\omega t}}{\omega^2 - \omega_{0,+}^2 + i\omega\Delta\omega_+}\begin{pmatrix} i\omega \\ i\alpha\omega - \omega_{2+} \end{pmatrix}\right], \\ \begin{pmatrix} X_- \\ Y_- \end{pmatrix} &= \text{Re}\left[\frac{2\gamma h_x \cos\theta e^{-i\omega t}}{\omega^2 - \omega_{0,-}^2 + i\omega\Delta\omega_-}\begin{pmatrix} i\alpha\omega - \omega_{1-} \\ -i\omega \end{pmatrix}\right],\end{aligned} \tag{10}$$

assuming $\alpha \ll 1$. Here, h_x and h_y are the x and y components of the oscillating field $\vec{h}_{\sim}$, $\omega_{1\pm} = \omega_{\text{eq}} \pm \omega_J$, $\omega_{2\pm} = \omega_{\text{eq}} \mp \omega_J\cos 2\theta - \omega_k\sin^2\theta$, and $\Delta\omega_\pm = \alpha(\omega_{1\pm} + \omega_{2\pm})$. An important inference to make from Eq. (9) is that the magnetization dot product has both quadratic and linear terms in the collective coordinates. This implies that the charge dynamics can have response at both ω and 2ω, where ω is the excitation

TABLE I. CrI_3 Parameters used in calculations.

Parameter	Value
Saturation magnetization, M_s [24]	1.37×10^{-5} emu/cm^2
Easy-axis anisotropy, K [24]	0.256 erg/cm^2
Interlayer exchange, $J_\perp$ [37]	0.035 erg/cm^2
Spin-charge coupling, λ [22]	1 mV
Area of bilayer CrI_3, A	1 μm^2

field frequency. We next analyze key experimental signatures of the proposed charge pumping.

IV. CHARGE DYNAMICS SIGNATURES

We begin by discussing the charge pumping in the absence of the external dc field $H = 0$ when the canting angle $\theta = 0$. In Fig. 3(a), we plot the amplitude of the charge current pumped as a function of the excitation frequency of external radiation, which is obtained by substituting the numerical solution of Eq. (7) into Eq. (6). Here, the AFMR are the well-known Kittel modes $\omega_{\rm Kittel} = \gamma\sqrt{H_k(H_k + 2H_J)}$ [36], which could be excited via a circular or linearly polarized radiation. We emphasize first that when exposed to circularly polarized oscillatory fields, i.e., $\vec{h}_\sim = h(\hat{x} \pm i\hat{y})/\sqrt{2}$, the eigenmodes do not lead to any charge dynamics (i.e., $\partial_t \vec{m}_1 \cdot \vec{m}_2 = 0$). This is because in this case the magnetizations of the two layers precess, keeping the angle between the magnetizations constant. On the other hand, in the presence of linearly polarized excitation fields, there is observable charge dynamics. Furthermore, from Eq. (9) we see that in the absence of external field (i.e., when $\theta = 0$), only quadratic terms in the magnetization dot product exist. Thus, the lowest-order charge dynamics arising from the magnetization dynamics for $H = 0$ has a response at twice the excitation frequency ($I^{2\omega}_{\rm amp}$) which at resonance ($\omega = \omega_{0,-}$) is approximately given by

$$I^{2\omega}_{\rm amp} \approx 2\lambda A C_{\rm g} \frac{\gamma^2 h_x^2 \left(\omega_{1-}^2 + \omega_{0,-}^2\right)}{\omega_{0,-}\Delta\omega_-^2}, \tag{11}$$

which is in agreement with the amplitude evaluated from the numerical solution of Eq. (7) plotted in Fig. 3(a).

A larger current response is generated in the presence of a dc canting field. This can be seen from Eq. (9), where due to nonzero θ we obtain a contribution to the charge current of the form $\sim \sin 2\theta\, \partial_t X_-$. This contribution, being linear in deviation, pumps a larger charge current (compared to the $H = 0$ case) oscillating at the frequency of incident radiation. The on-resonance ($\omega = \omega_{0,-}$) amplitude of charge current can be approximated from Eq. (9) and Eq. (10), given by

$$I^{\omega}_{\rm amp} \approx 2\lambda A C_{\rm g} \sin 2\theta \cos\theta \frac{2\gamma h_x \sqrt{\omega_{1-}^2 + \alpha^2\omega_{0,-}^2}}{\Delta\omega_-}. \tag{12}$$

In Fig. 3(b), we plot the amplitude of this current ($I^{\omega}_{\rm amp}$) as a function of in-plane dc magnetic field and excitation frequency for an x-polarized oscillating magnetic field evaluated from substituting the numerical solution of Eq. (7) into Eq. (6). The linear response estimate in Eq. (12) agrees with the numerical result. The linear term contribution $\sin 2\theta\, \partial_t X_- \sim \omega \sin 2\theta\, X_-$ peaks at an intermediate canting angle, arising from the angular dependence $\sin 2\theta$ which varies from $\theta = 0$ (at $H = 0$) to $\theta = \pi/2$ (at $H = H_k + 2H_J$). For typical experimentally realized values of the parameters (see Table I), this peak current gives a value of $\sim$3 nA per Oe of oscillating magnetic field for micron-sized flakes (that have monodomain ground state [20,38]), well within the reach of experiments.

V. CONCLUSIONS AND OUTLOOK

In this paper, we constructed a phenomenological theory for coupled spin-charge dynamics in symmetrically gated vdW heterostructures of bilayer CrI_3. We find that the spin-charge coupling can be classified into doping-induced modifications of magnetic properties and the so-called magnetoelectric coupling, which represents the interaction of electric field with the difference of magnetizations in each layer. The structural symmetries restrict the form of the former (latter) to be directly proportional to the symmetric (antisymmetric) combination of charge doping within each layer. Motivated by the experimental observation of large doping-induced changes in interlayer exchange coupling, we specifically construct an effective circuit theory for coupled spin-charge dynamics including this term, which if needed can similarly be extended to include other spin-charge couplings.

A central finding of this theory is that the magnetization dynamics induces a voltage, which is proportional to the dot product of magnetizations within each layer. As an experimental signature of this effect, we proposed and evaluated the charge current pumped by magnetization dynamics induced by the absorption of electromagnetic radiation. This can be utilized for probing magnetic excitations electrically, in addition to tunneling magnetoresistance [23], and harvesting electromagnetic radiation via conversion into an electrical signal with the following features. In the absence of any dc magnetic field, the resulting charge dynamics have a response at twice the excitation field frequency when exposed to linearly polarized time-dependent electromagnetic fields. These high-frequency AFMR modes can be softened by applying a dc magnetic field, which additionally allows a first harmonic response when a time-dependent electromagnetic field is polarized along the dc field direction. In addition to the harmonic charge dynamics response, there is also a dc voltage $\sim(\vec{m}_1 \cdot \vec{m}_2)$. This could in principle be measured, for example, by artificially adding a very large resistance in the external circuit of Fig. 1 and modulating the microwave power (at frequency larger than the $1/RC_g$). The corresponding modulated voltage could be measured as a small current flowing through the external resistor R. This could act as a subterahertz microwave detector.

Future works should explore the implications and opportunities offered by the reciprocity dictated pair of "voltage $\leftrightarrow$ magnetization dynamics" in addition to the proposed AFMR setup. For example, thanks to the easy integration of various vdW materials, spin transistors have recently been fabricated [39]. Here, a gate-voltage-dependent magnetic configuration of bilayer CrI_3 controls the flow of tunneling charge current due to the tunneling magnetoresistance and through shift in the chemical potential of the vdW layers. Solving coupled spin-charge circuits in such vdW magnet-based spin transistors will be addressed elsewhere.

ACKNOWLEDGMENTS

We thank Vaibhav Ostwal, Se Kwon Kim, and Kin Fai Mak for helpful discussions. A.R., A.S., and P.U. acknowledge support from the National Science Foundation through Grant No. DMR-1838513. Collaboration with Y.T. was supported by the National Science Foundation through Grant No. ECCS-1810494.

[1] K. S. Burch, D. Mandrus, and J.-G. Park, Nature (London) **563**, 47 (2018).

[2] M. Gibertini, M. Koperski, A. F. Morpurgo, and K. S. Novoselov, Nat. Nanotechnol. **14**, 408 (2019).

[3] C. Gong, L. Li, Z. Li, H. Ji, A. Stern, Y. Xia, T. Cao, W. Bao, C. Wang, Y. Wang *et al.*, Nature (London) **546**, 265 (2017).

[4] A. K. Geim and I. V. Grigorieva, Nature (London) **499**, 419 (2013).

[5] I. Žutić, J. Fabian, and S. Das Sarma, Rev. Mod. Phys. **76**, 323 (2004).

[6] W. Han, Y. Otani, and S. Maekawa, npj Quantum Mater. **3**, 27 (2018).

[7] L. Berger, Phys. Rev. B **54**, 9353 (1996).

[8] J. C. Slonczewski, J. Magn. Magn. Mater. **159**, L1 (1996).

[9] Y. Tserkovnyak, A. Brataas, G. E. W. Bauer, and B. I. Halperin, Rev. Mod. Phys. **77**, 1375 (2005).

[10] P. Vaidya, S. A. Morley, J. van Tol, Y. Liu, R. Cheng, A. Brataas, D. Lederman, and E. Del Barco, Science **368**, 160 (2020).

[11] M. Dyakonov and V. Perel, Phys. Lett. A **35**, 459 (1971).

[12] E. Saitoh, M. Ueda, H. Miyajima, and G. Tatara, Appl. Phys. Lett. **88**, 182509 (2006).

[13] T. Kimura, Y. Otani, T. Sato, S. Takahashi, and S. Maekawa, Phys. Rev. Lett. **98**, 156601 (2007).

[14] J. Sinova, S. O. Valenzuela, J. Wunderlich, C. H. Back, and T. Jungwirth, Rev. Mod. Phys. **87**, 1213 (2015).

[15] V. M. Edelstein, Solid State Commun. **73**, 233 (1990).

[16] H. J. Zhang, S. Yamamoto, B. Gu, H. Li, M. Maekawa, Y. Fukaya, and A. Kawasuso, Phys. Rev. Lett. **114**, 166602 (2015).

[17] J. R. Sánchez, L. Vila, G. Desfonds, S. Gambarelli, J. Attané, J. De Teresa, C. Magén, and A. Fert, Nat. Commun. **4**, 2944 (2013).

[18] M. Fiebig, J. Phys. D: Appl. Phys. **38**, R123 (2005).

[19] J. Zhang, C. Fang, and G. J. Weng, Proc. R. Soc. London Ser. A **475**, 20190002 (2019).

[20] B. Huang, G. Clark, E. Navarro-Moratalla, D. R. Klein, R. Cheng, K. L. Seyler, D. Zhong, E. Schmidgall, M. A. McGuire, D. H. Cobden *et al.*, Nature (London) **546**, 270 (2017).

[21] N. Sivadas, S. Okamoto, X. Xu, C. J. Fennie, and D. Xiao, Nano Lett. **18**, 7658 (2018).

[22] S. Jiang, L. Li, Z. Wang, K. F. Mak, and J. Shan, Nat. Nanotechnol. **13**, 549 (2018).

[23] D. R. Klein, D. MacNeill, J. L. Lado, D. Soriano, E. Navarro-Moratalla, K. Watanabe, T. Taniguchi, S. Manni, P. Canfield, J. Fernández-Rossier *et al.*, Science **360**, 1218 (2018).

[24] J. L. Lado and J. Fernández-Rossier, 2D Mater. **4**, 035002 (2017).

[25] Furthermore, terms of the form $\sim(\sigma_1+\sigma_2)m_{i,z}^2$, i.e., doping-induced change in uniaxial ansiotropy, are also allowed. However, motivated by the experimental observation that the percentage change in anisotropy is typically smaller than that in the exchange interaction, i.e., $\Delta K/K \ll \Delta J/J$ [22], we have not included those here.

[26] J. Zhu, J. A. Katine, G. E. Rowlands, Y.-J. Chen, Z. Duan, J. G. Alzate, P. Upadhyaya, J. Langer, P. K. Amiri, K. L. Wang, and I. N. Krivorotov, Phys. Rev. Lett. **108**, 197203 (2012).

[27] T. Nozaki, Y. Shiota, S. Miwa, S. Murakami, F. Bonell, S. Ishibashi, H. Kubota, K. Yakushiji, T. Saruya, A. Fukushima *et al.*, Nat. Phys. **8**, 491 (2012).

[28] The strength of VCMA is characterized as $\Delta K_i = \nu\sigma$, where interfacial charge (per unit area) σ couples to the magnetic order by modifying the interfacial perpendicular anisotropy energy (per unit area) K_i. The coupling ν is typically $\sim$mV [26].

[29] In addition, charges also give rise to electrostatic energy stored in the vdW gap between the graphene contact and the CrI_3 layer (parametrized by $C_{g,gc}$), as well as the chemical energy due to shifts in the Fermi levels of the graphene contacts and the CrI_3 layers (parametrized by the quantum capacitances C_{qg} and C_{qc}, respectively). However, for typical experimental parameters we have $C_g \ll C_{qg} \sim C_{g,gc} \ll C_{qc}$. Thus, the electrical energy is dominated by the one stored in the electrostatic fields in the h-BN layer [22].

[30] The lumped-circuit assumption is valid for length scales set by the wavelength of lateral electromagnetic waves propagating within the heterostructure $2\pi/(\omega\sqrt{L_l C_l}) \sim 10$–$100\ \mu$m (where $C_l = \varepsilon_0\varepsilon_r w/d \sim 10^{-7}$ F/m and $L_l = \mu_0\mu_r d/w \sim 10^{-5}$–$10^{-7}$ H/m are the capacitance and inductance per unit length of the heterostructure of width w and effective distance between layers, d).

[31] To estimate the contact resistance at the graphene-CrI_3 interface, we can consider typical contact resistance associated with graphene–transition metal dichalcogenide [32, 33] interfaces for micron-sized systems R_{contact} Area $\sim 1000\ \Omega\,\mu\text{m}^2$.For typical h-BN thicknesses, the geometric capacitance per unit area $C_g \approx 10^{-7}$ F/cm^2 [34]. Neglecting the external circuit resistance, the time constant associated with the circuit is R_{contact} Area $\times\, C_g \approx 1$ ps.

[32] M. Houssa, K. Iordanidou, A. Dabral, A. Lu, R. Meng, G. Pourtois, V. Afanas' ev, and A. Stesmans, Appl. Phys. Lett. **114**, 163101 (2019).

[33] T. Yamaguchi, R. Moriya, Y. Inoue, S. Morikawa, S. Masubuchi, K. Watanabe, T. Taniguchi, and T. Machida, Appl. Phys. Lett. **105**, 223109 (2014).

[34] Z. Wang, Y.-H. Chiu, K. Honz, K. F. Mak, and J. Shan, Nano Lett. **18**, 137 (2017).

[35] S. V. Von Sovskii, *Ferromagnetic Resonance: The Phenomenon of Resonant Absorption of a High-Frequency Magnetic Field in Ferromagnetic Substances* (Elsevier, Amsterdam, 2016).

[36] F. Keffer and C. Kittel, Phys. Rev. **85**, 329 (1952).

[37] D. Soriano, C. Cardoso, and J. Fernández-Rossier, Solid State Commun. **299**, 113662 (2019).

[38] L. Thiel, Z. Wang, M. A. Tschudin, D. Rohner, I. Gutiérrez-Lezama, N. Ubrig, M. Gibertini, E. Giannini, A. F. Morpurgo, and P. Maletinsky, Science **364**, 973 (2019).

[39] S. Jiang, L. Li, Z. Wang, J. Shan, and K. F. Mak, Nat. Electron. **2**, 159 (2019).